XII International Conference on Computational Plasticity. Fundamentals and Applications
COMPLAS XII
E. Oñate, D.R.J. Owen, D. Peric and B. Suárez (Eds)

NUMERICAL SOLUTION OF PERFECT PLASTIC PROBLEMS WITH CONTACT: PART II - NUMERICAL REALIZATION

MARTIN CERMAK[*,‡], JAROSLAV HASLINGER[†,‡], STANISLAV SYSALA[‡]

[*]VŠB–Technical University of Ostrava
IT4Innovations
17. listopadu 15, 708 33 Ostrava, Czech Republic
e-mail: martin.cermak@vsb.cz, web page: http://www.vsb.cz

[†]Charles University in Prague
Department of Numerical Mathematics, Faculty of Mathematics and Physics
Sokolovská 83, 186 75 Prague, Czech Republic
e-mail: hasling@karlin.mff.cuni.cz, web page: http://www.mff.cuni.cz

[‡]Institute of Geonics AS CR, v.v.i.
Department of IT4Innovations
Studentská 1768, 708 00 Ostrava, Czech Republic
e-mail: stanislav.sysala@ugn.cas.cz, web page: http://www.ugn.cas.cz

Key words: Perfect plasticity, Contact, Domain decomposition

Abstract. This contribution is a continuation of our contribution denoted as PART I, where the discretized contact problem for elasto-perfectly plastic bodies was studied and suitable numerical methods were introduced. In particular, frictionless contact boundary conditions and Hencky's material model with the von Mises criterion are considered. Here we describe some implementation details and present several numerical examples.

1 INTRODUCTION

This contribution is a continuation of PART I ([2]). We briefly describe some implementation details and present several numerical examples. Some of the results will appear in [3].

Algorithms ALG1-ALG4 introduced in PART I ([2]) have a common feature: in each iteration it is necessary to solve a quadratic programming problem. For numerical realization of this inner problem, we use a combination of the TFETI domain decomposition method [5] and the SMALSE-M method [6], similarly as in [1, 4]. The whole contact problem for elastic-perfectly plastic bodies is implemented in MatLab within the MatSol

library [8]. Another approach for numerical realization of contact problems for elasto-plastic bodies can be found in [10].

This contribution is organized as follows. The algebraic formulation of the discretized problem is introduced in Section 2. In Section 3, some details concerning numerical realization of the inner problem are mentioned. In Section 4, numerical results of several model examples for elasto-perfectly plastic problems (with and without contact) are presented. Concluding remarks can be found in Section 5.

2 ALGEBRAIC FORMULATION OF THE PROBLEM

In accordance with PART I ([2]), we consider two polyhedric domains $\Omega^1, \Omega^2 \subseteq \mathbb{R}^3$, whose boundaries are decomposed as follows: $\partial\Omega^j = \overline{\Gamma}_u^j \cup \overline{\Gamma}_f^j \cup \overline{\Gamma}_c^j$, $j = 1, 2$, where Γ_u^j, Γ_f^j, Γ_c^j are open and mutually disjoint. On $\Gamma_u^j \neq \emptyset$, the structure is fixed, while surface tractions are applied on Γ_f^j, $j = 1, 2$. Further, $\Gamma_c := \Gamma_c^1 = \Gamma_c^2$ is a bounded contact zone, where the frictionless contact boundary conditions are prescribed.

Since we apply the TFETI domain decomposition method [5], we decompose Ω^1 and Ω^2 into disjoint polyhedric subdomains $\Omega^{j,p} \subset \Omega^j$, $p = 1, 2, \ldots, s_j$, $j = 1, 2$, see Figure 1. Continuity of a solution between two adjacent subdomains and the satisfaction of the Dirichlet condition will be taken into account by adding equality constraints into the definition of $\mathcal{K}$, see below.

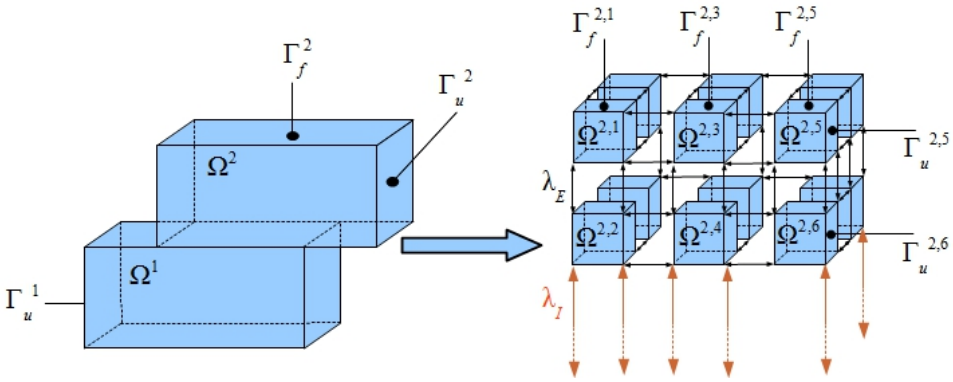

Figure 1: Scheme of the geometry and domain decomposition

Let $\mathcal{T}_h^{j,p}$ be a regular partition of $\overline{\Omega}^{j,p}$, $j = 1, 2$, $p = 1, 2, \ldots, s_j$, into tetrahedrons such that the nodes on the contact and common parts of boundaries of two adjacent subdomains coincide. On any $\Omega^{j,p}$, we construct the spaces of continuous and piecewise linear displacements over $\mathcal{T}_h^{j,p}$. Thus any global displacement vector $\mathbf{v} \in \mathbb{R}^n$ has the following structure

$$\mathbf{v} = \left(\mathbf{v}_{1,1}^T, \mathbf{v}_{1,2}^T, \ldots, \mathbf{v}_{1,s_1}^T, \mathbf{v}_{2,1}^T, \ldots, \mathbf{v}_{2,s_2}^T\right)^T,$$

where $\mathbf{v}_{j,p}$ denotes the displacement vector on $\Omega^{j,p}$, $j = 1, 2$, $p = 1, 2, \ldots, s_j$. Furthermore, the set of kinematically admissible displacement vectors is given by

$$\mathcal{K} := \{\mathbf{v} \in \mathbb{R}^n \mid \mathbf{B}_E\mathbf{v} = \mathbf{o},\ \mathbf{B}_I\mathbf{v} \leq \mathbf{o}\}\,.$$

By means of the matrix $\mathbf{B}_E \in \mathbb{R}^{m_E \times n}$, we express the gluing conditions among neighboring subdomains and the satisfaction of the homogeneous Dirichlet boundary condition, while the matrix $\mathbf{B}_I \in \mathbb{R}^{m_I \times n}$ is used to express the non-penetration condition on Γ_c.

The algebraic formulation of problem $(\mathcal{P})_{h,\zeta}$, $\zeta \geq 0$, introduced in PART I ([2]) reads as follows:

$$\text{find } \mathbf{u} \in \mathcal{K}: \quad \begin{cases} J_\zeta(\mathbf{u}) \leq J_\zeta(\mathbf{v}) & \forall \mathbf{v} \in \mathcal{K}, \\ J_\zeta(\mathbf{v}) := \Psi(\mathbf{v}) - \zeta \mathbf{f}^T\mathbf{v}, & \mathbf{v} \in \mathbb{R}^n. \end{cases}$$

Here $\mathbf{f} = \left(\mathbf{f}_{1,1}^T, \ldots, \mathbf{f}_{1,s_1}^T, \mathbf{f}_{2,1}^T, \ldots, \mathbf{f}_{2,s_2}^T\right)^T \in \mathbb{R}^n$ is the load vector corresponding to the applies volume and surface forces. The function Ψ is the algebraic form of the inner energy functional and has the following structure:

$$\Psi(\mathbf{v}) = \left(\Psi_{1,1}(\mathbf{v}_{1,1})^T, \ldots, \Psi_{1,s_1}(\mathbf{v}_{1,s_1})^T, \Psi_{2,1}(\mathbf{v}_{2,1})^T, \ldots, \Psi_{2,s_2}(\mathbf{v}_{2,s_2})^T\right)^T.$$

Similarly, one can rewrite problems $(\mathcal{P})^*_{h,\zeta}$, $(\mathcal{S})_{h,\zeta,r}$, $(\mathcal{S})^\alpha_h$, $(\mathcal{P})^\alpha_h$ introduced in PART I ([2]) into the algebraic form.

3 NOTES TO NUMERICAL REALIZATION OF INNER PROBLEMS

As we have mentioned, algorithms ALG1-ALG4 introduced in PART I ([2]) lead to the quadratic programming problems in each iteration. The scheme of these inner subproblems solved in the k-th iterative step is the following:

$$\text{find } \mathbf{u}^k \in \mathcal{K}_k: \quad J_k(\mathbf{u}^k) \leq J_k(\mathbf{v}) \qquad \forall \mathbf{v} \in \mathcal{K}_k, \tag{1}$$

where

$$J_k(\mathbf{v}) := \frac{1}{2}\mathbf{v}^T\mathbf{K}_k^\rho\mathbf{v} - \mathbf{f}_k^T\mathbf{v}, \quad \mathbf{v} \in \mathcal{K}_k, \tag{2}$$

and

$$\mathcal{K}_k := \left\{\mathbf{v} \in \mathbb{R}^n\ ;\ \tilde{\mathbf{B}}_E\mathbf{v} = \mathbf{c}_{E,k},\ \mathbf{B}_I\mathbf{v} \leq \mathbf{c}_{I,k}\right\}.$$

Here $\mathbf{K}_k^\rho \in \mathbb{R}^{n\times n}$ is a symmetric and positive semidefinite matrix representing the function $\Sigma^{o,\rho}(u^k)$, $\rho \in [0, 1]$, introduced in PART I ([2]). Let us recall that $\Sigma^{o,1}(u^k) = C$, i.e. we obtain the elastic stiffness matrix for $\rho = 1$ (see ALG2). The computed vector $\mathbf{u}^k$ represents either δu^k in ALG1, ALG3, ALG4, or u^k in ALG2. The form of the load vector $\mathbf{f}_k$ depends on the particular algorithm, but always it contains $\mathbf{f}$. For ALG1, ALG2, ALG4, it holds that $\tilde{\mathbf{B}}_E = \mathbf{B}_E$ and $\mathbf{c}_{E,k} = \mathbf{o}$. For ALG3, the contraints $L(v) = \alpha$ is additionally included into $\tilde{\mathbf{B}}_E\mathbf{v} = \mathbf{c}_{E,k}$.

The TFETI domain decomposition method has been analyzed e.g. in [5, 6, 7]. All constraints appearing in the definition of $\mathcal{K}_k$ will be released by using Lagrange multipliers, see Figure 1. In particular, we use two types of the Lagrange multipliers, namely $\boldsymbol{\lambda}_I \in \mathbb{R}^{m_I}$, $\boldsymbol{\lambda}_I \geq \mathbf{o}$ related to the inequality constraints, and $\boldsymbol{\lambda}_E \in \mathbb{R}^{\tilde{m}_E}$ related to the equality constraints. To simplify our notation, we denote

$$\boldsymbol{\lambda} = \begin{bmatrix} \boldsymbol{\lambda}_E \\ \boldsymbol{\lambda}_I \end{bmatrix}, \quad \mathbf{B} = \begin{bmatrix} \tilde{\mathbf{B}}_E \\ \mathbf{B}_I \end{bmatrix}, \quad \mathbf{c}_k = \begin{bmatrix} \mathbf{c}_{E,k} \\ \mathbf{c}_{I,k} \end{bmatrix},$$

and

$$\Lambda = \{\boldsymbol{\lambda} = (\boldsymbol{\lambda}_E^T, \boldsymbol{\lambda}_I^T)^T \in \mathbb{R}^{\tilde{m}_E + m_I} : \ \boldsymbol{\lambda}_I \geq \mathbf{o}\}.$$

Then the Lagrangian associated with (1) reads as

$$L_k(\mathbf{v}, \boldsymbol{\lambda}) = \frac{1}{2}\mathbf{v}^T \mathbf{K}_k^\rho \mathbf{v} - \mathbf{f}_k^T \mathbf{v} + \boldsymbol{\lambda}^T(\mathbf{B}\mathbf{v} - \mathbf{c}_k), \quad \mathbf{v} \in \mathbb{R}^n, \ \boldsymbol{\lambda} \in \Lambda. \tag{3}$$

Using convexity of L_k and of the constraints, we can use the classical duality theory to reformulate problem (1) to get

$$J_k(\mathbf{u}^k) = \min_{\mathbf{v} \in \mathcal{K}_k} J_k(\mathbf{v}) = \min_{\mathbf{v} \in \mathbb{R}^n} \sup_{\boldsymbol{\lambda} \in \Lambda} L_k(\mathbf{v}, \boldsymbol{\lambda}) = \max_{\boldsymbol{\lambda} \in \Lambda} \inf_{\mathbf{v} \in \mathbb{R}^n} L_k(\mathbf{v}, \boldsymbol{\lambda}). \tag{4}$$

The max-inf problem in (4) is solved by algorithm SMALSE-M [6]. This algorithm is based on the active set strategy and it combines three steps: CG with preconditioning based on orthogonal projectors, expansion, and proportioning.

4 NUMERICAL EXPERIMENTS

In this section, we illustrate the efficiency of the proposed algorithms on several model examples. First, we will apply ALG1, ALG2 and ALG3 to a model contact problem for two bodies. Then we will compare the loading paths computed by ALG1, ALG3 and ALG4 for a plane strain problem considering only one body without the contact boundary conditions.

4.1 3D contact problem

Let Ω^1 and Ω^2 be two $(3000 \times 1000 \times 1000)$ blocks with the configuration seen in Figure 1. Observe that Ω^1, Ω^2 are fixed along the left, and right lateral face, respectively. The contact zone occupies 80% of the area of the faces. The load L is represented by the constant surface traction $f = (0, 0, 100)$ acting on the upper face of Ω^2 and corresponds to $\zeta = 1$. Ω^1 and Ω^2 are decomposed into 24 subdomains. The mesh $\mathcal{T}_h$ contains 6 000 nodes and 18 434 tetrahedrons. Both bodies Ω^i are made of the same elasto-perfectly plastic material which is characterized by the Young modulus $E = 206\,900$, the Poisson ratio $\nu = 0.29$ and $\gamma = 450\sqrt{2/3}$ representing the initial yield stress.

In the first set of numerical experiments, we investigate convergence of ALG1 and ALG2 in dependence on ζ, ρ, and r, respectively. In particular, we initiate ALG1,2 using the zero displacements, strain and stress vectors and choose the stopping criterion given by the relative displacement error (see PART I [2]) with the tolerance $\epsilon_u = 1e-4$.

For ALG1, the dependence of number of iterations on ζ and ρ is shown in Table 1.

Table 1: Number of iterations in dependence on ζ and ρ for ALG1

$\zeta \setminus \rho$	0.00	0.05	0.10	0.15	0.20	0.30	0.50	1.00
1.00	5	5	6	6	6	7	8	10
1.30	7	11	13	16	18	24	30	48
1.50	11	41	65	87	107	143	205	331

One can observe that the smallest number of iterations is for $\rho = 0$ and this number increases with increasing ζ and ρ. On the other hand, if we use ALG1 without damping, then convergence for $\rho = 0$ is problematic for higher values of ζ. But the influence of damping turns out to be minimal for $\rho > 0$.

If ALG2 is used, convergence is faster for r between 0.10 and 0.30 independently of ζ. Moreover for $r < 0.05$ or $r > 0.50$ and higher values of ζ, convergence is too slow.

The stress and displacement fields obtained by ALG1 and ALG2 are very similar. Furthermore, the results obtained for other stopping criteria mentioned in PART I ([2]) are also similar.

In the second set of experiments we compare the loading paths obtained by ALG1, ALG2 and ALG3 for the fixed values $r = 0.2$, $\rho = 0$ and $\rho = 0.1$.

For ALG1,2, we use adaptively chosen values of ζ:

$$0 = \zeta_0 < \zeta_1 < \zeta_2 < \ldots < \zeta_i < \ldots < \zeta_N.$$

The increments $\triangle\zeta_i := \zeta_i - \zeta_{i-1}$ decrease for increasing i and are determined in dependence on convergence of ALG1,2. For any $i = 1, 2, \ldots$, the corresponding displacements u_i and the values $\alpha_i = L(u_i)$ are computed. ALG1 is initiated by using the zero displacements for $\rho = 0$ and u_{i-1} for $\rho = 0.1$. Let us note that the initial choice u_{i-1} for $\rho = 0$ leads to the loss of convergence for larger i. ALG2 is initiated by using the zero strain and stress vectors for any $i = 1, 2, \ldots$. Further, we use the stopping criterion given by the relative displacement error with the tolerance $\epsilon_u = 1e-4$. The loading process terminates if $\alpha_i > 7e9$ for some i. This value of α is sufficiently large to estimate ζ_{lim}, see Figure 2.

For ALG3 we use $\rho = 0$. In the loading process, we keep the constant increment $\triangle\alpha = \alpha_{el}/2 \approx 0.27e9$, where α_{el} is the maximal value of α, for which the solution to $(\mathcal{P})_h^\alpha$ coincides with the solution to the corresponding contact problem for elastic bodies, see the circle in Figure 2. Then α increases up to the value $7e9$. For a fixed value of α_i,

$i = 1, 2, \ldots$, we use the same stopping criterion and the tolerance as in ALG1,2. Algorithm ALG3 is iniciated using u_{i-1} computed in the previous step.

The comparison of the loading paths for all ALG1-ALG3 is shown in Figure 2.

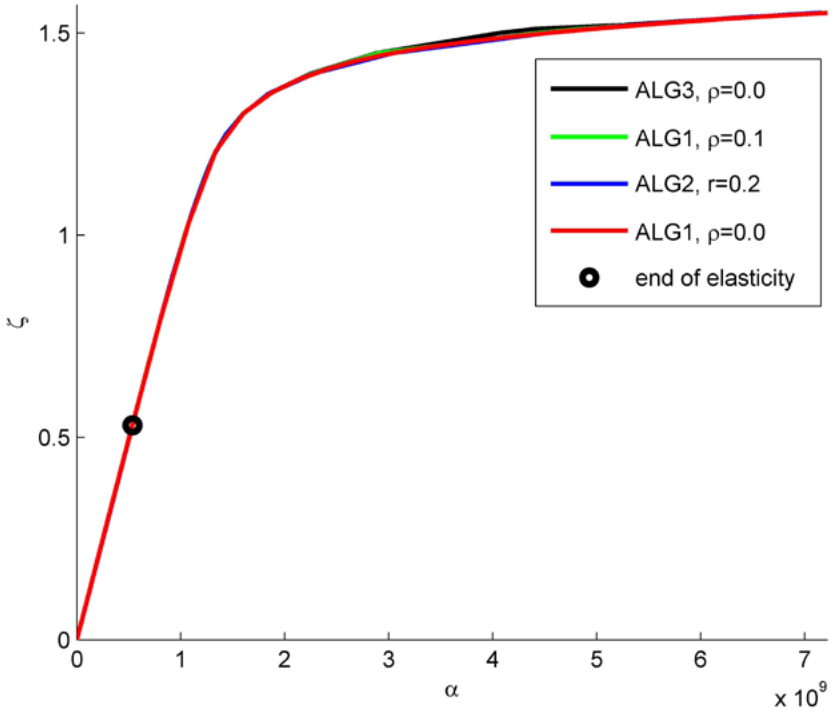

Figure 2: Comparison of loading paths.

One can see that the curves practically coincide. They are increasing and $\zeta_{lim} \approx 1.55$. Notice that ALG3 converges here even for $\rho = 0$. This does not hold for ALG1.

Finally, the stress and displacements fields at the end of the loading process are depicted in Figure 3 and 4, respectively. From Figure 3 on the left, one can detect plastic parts of the bodies, where the maximal value $\gamma = 450\sqrt{2/3}$ is attained. From the right picture, one can observe possible shear zones in the vicinity of the fixed parts of the bodies.

4.2 Plane strain problem without contact

The configuration of a 2D domain Ω is as Figure 5. On the left and bottom parts of its boundary, we prescribe the homogeneous Dirichlet boundary conditions only in the normal direction, i.e. the symmetry conditions are prescribed. On the top of the domain, the surface traction in the normal direction is applied. The elasto-perfectly plastic material is considered and characterized by the Young modulus $E = 206\,900$, the Poisson ratio

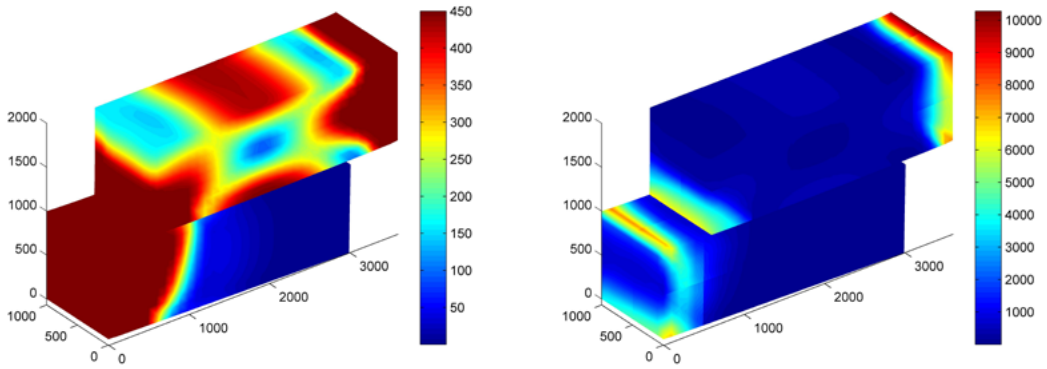

Figure 3: Von Mises stress for σ (left) and $C\varepsilon(u)$ (right) at the end of the loading process.

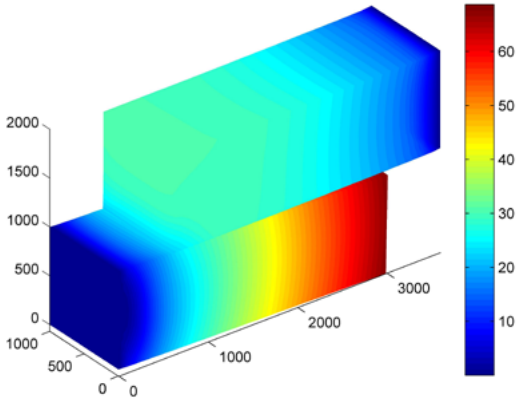

Figure 4: Displacements at the end of the loading process.

$\nu = 0.29$ and $\gamma = 450\sqrt{2/3}$.

First, we compare the loading paths obtained by ALG1 ($\rho = 0$), ALG3 ($\rho = 0.1$) and ALG4 ($\rho = 0$) for fixed ρ similarly as in the previous example. To this end, we use the mesh with 7600 elements and 3927 nodal points. Again, the obtained curves practically coincide, see Figure 6.

Notice that we could not use ALG3 with $\rho = 0$ for determining the whole loading path due to loss of convergence. Moreover, for $\rho = 0.1$, ALG4 is a little bit faster than ALG3.

Secondly, we will compare the loading paths in dependence on the discretization parameter h. To this end, we use ALG3 with $\rho = 0.1$ for three different meshes with 3960, 7600 and 20664 elements. The corresponding loading paths for $\alpha \in \langle 0, 1008 \rangle$ are shown in Figure 7. The computed values of ζ corresponding to $\alpha = 1008$ are 1.077, 1.066, and

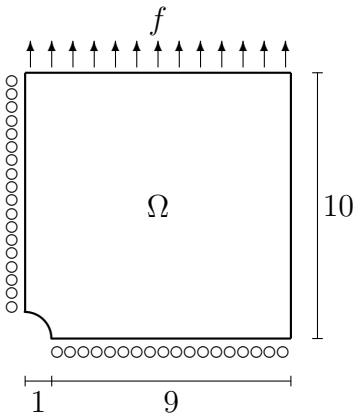

Figure 5: Geometry of the problem.

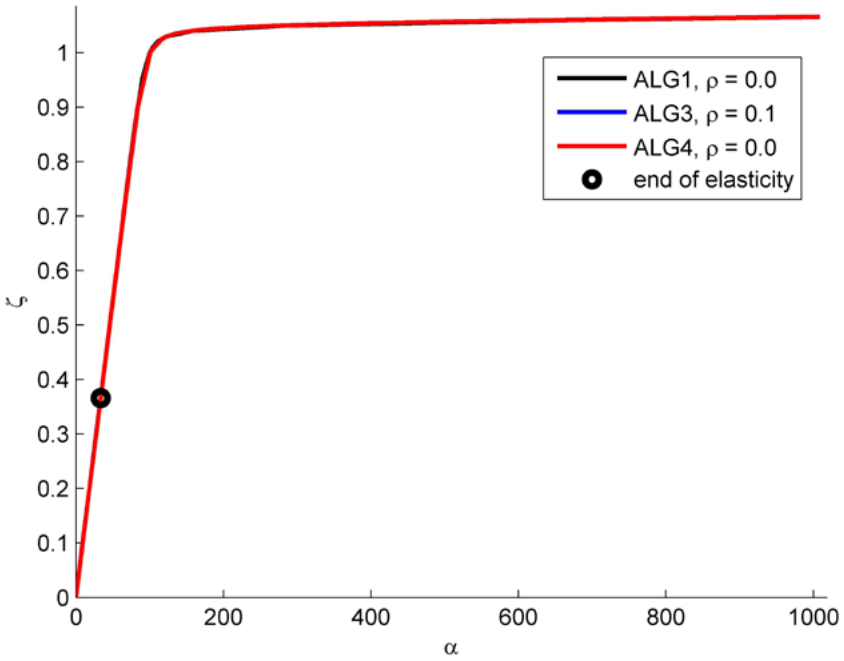

Figure 6: Comparison of loading paths.

1.055, respectively. It means that the values of the limit load parameter decrease with decreasing h, which is in accordance with the expected theoretical results.

Finally, we illustrate the stress and displacement states at the end of the loading process, see Figure 8 and 9.

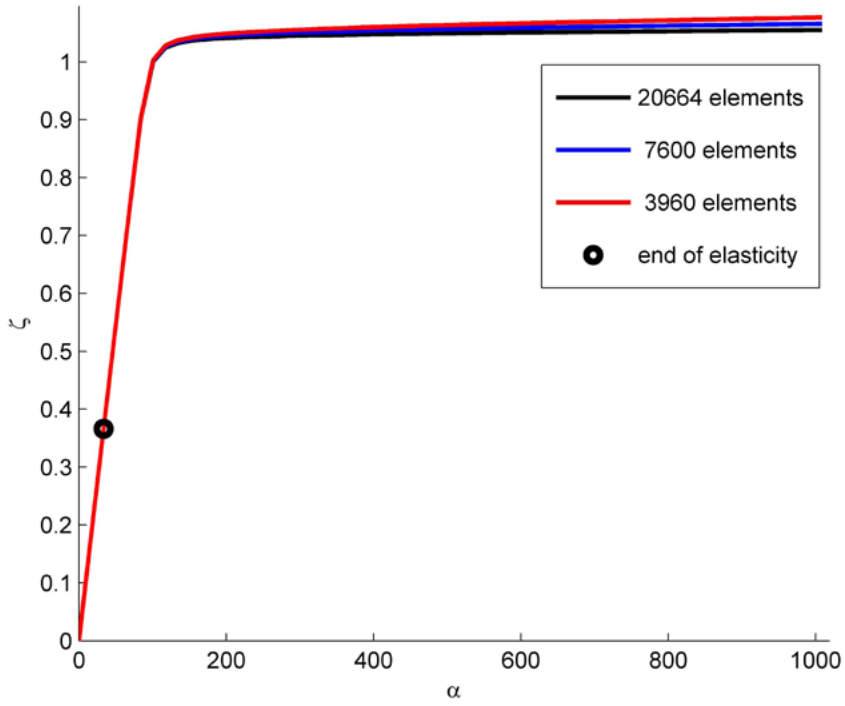

Figure 7: Comparison of loading paths in dependence on the discretization parameter.

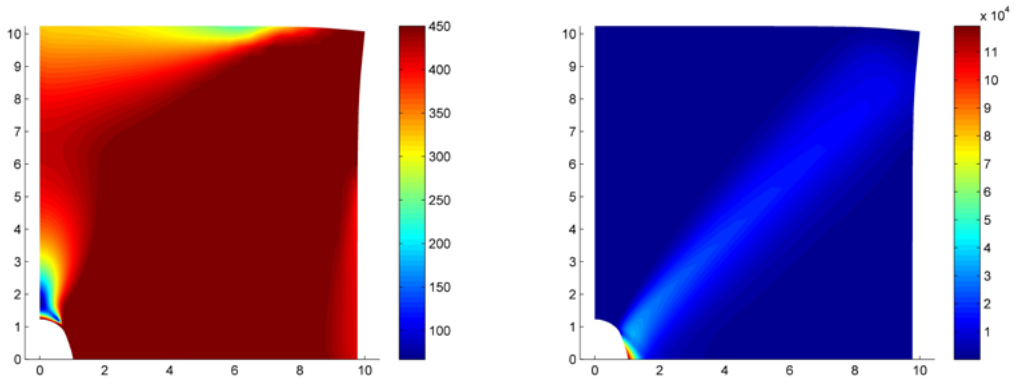

Figure 8: Von Mises stress for σ (left) and $C\varepsilon(u)$ (right) at the end of the loading process.

5 CONCLUSIONS

This contribution deals with numerical realization of ALG1-ALG4, which were introduced in PART I ([2]) as possible tools for solving elasto-perfectly plastic contact problems.

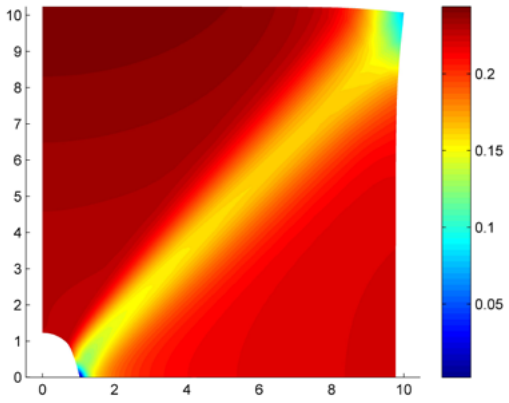

Figure 9: Displacement at the end of the loading process.

The efficiency of the algorithms was tested on several model examples.

We see that convergence of ALG2 depends on the parameter r appearing in the augmented Lagrangian. However it is not clear how to find an optimal value of r. Further, we analyzed how the regularization parameter ρ influences convergence of ALG1, ALG3 and ALG4. The smaller value of ρ is, faster convergence is. On the other hand, we found situations, when the choice $\rho = 0$ led to loss of convergence for all of these algorithms.

We also compared two different strategies for controlling the loading process: or by the load parameter ζ or by the parameter α representing the work of external forces. Both strategies have some advantages and disadvantages. For example, numerical realization of $(\mathcal{P})_h^\alpha$ can be more complicated than for $(\mathcal{P})_{h,\zeta}$. On the other hand, $(\mathcal{P})_h^\alpha$ has a solution for any $\alpha \geq 0$ and thus controlling the process by α is simpler than by ζ.

Acknowledgments. This work was supported by the European Regional Development Fund in the IT4Innovations Centre of Excellence project (CZ.1.05/1.1.00/02.0070) and by the project SPOMECH - Creating a multidisciplinary R&D team for reliable solution of mechanical problems, reg. no. CZ.1.07/2.3.00/20.0070 within Operational Programme 'Education for competitiveness' funded by Structural Funds of the European Union and state budget of the Czech Republic.

REFERENCES

[1] Cermak, M.: *Scalable algorithms for solving elasto-plastic problems.* Ph.D. thesis, VSB-TU Ostrava (2012).

[2] Cermak, M., Haslinger, J., Sysala, S.: *Numerical solutions of perfect plastic problems with contact: PART I - theory.* Submitted as a contribution for Complas XII.

[3] Cermak, M., Haslinger, J., Kozubek, T., Sysala, S.: *Discretization and numerical realization of contact problems for elastic-perfectly plastic bodies. PART II – numerical realization, limit analysis.* To appear.

[4] Cermak, M., Kozubek, T., Sysala, S., Valdman J.: *A TFETI Domain Decomposition Solver for Elastoplastic Problems.* arXiv:1205.1926 [math.NA].

[5] Dostál, Z., Horák, D., Kučera, R.: *Total feti - an easier implementable variant of the feti method for numerical solution of elliptic pde.* Communications in Numerical Methods in Engineering. (2006) **22**: 1155–1162.

[6] Dostál, Z., Kozubek, T.: *An optimal algorithm and superrelaxation for minimization of a quadratic function subject to separable convex constraints with applications*, Mathematical Programming. (2012) **135**, 1-2: 195–220.

[7] Dostál, Z., Kozubek, T., Vondrák, V., Brzobohatý, T., Markopoulos, A.: *Scalable tfeti algorithm for the solution of multibody contact problems of elasticity.* International Journal for Numerical Methods in Engineering. (2012) **82**: 1384–1405.

[8] Kozubek, T., Markopoulos, A., Brzobohatý, T., Kučera, R., Vondrák, V., Dostál, Z.: *Matsol - matlab efficient solvers for problems in engineering.* Available from http://matsol.vsb.cz/ (2012).

[9] Sysala, S., Haslinger, J., Hlaváček, I., Cermak, M.: *Discretization and numerical realization of contact problems for elastic-perfectly plastic bodies. PART I – discretization, limit analysis.* Submitted.

[10] Wohlmuth, B.: *Variationally consistent discretization schemes and numerical algorithms for contact problems.* Acta Numerica (2011) **20**: 569–734.